

The 1992 Little Skull Mountain Earthquake Sequence, Southern Nevada Test Site

by Kenneth D. Smith, James N. Brune, Diane dePolo, Martha K. Savage,
Rasool Anooshehpour, and Anne F. Sheehan

Abstract The M_L 5.6–5.8 Little Skull Mountain, Nevada, 29 June 1992 earthquake occurred in the southwest portion of Nevada Test Site (NTS) approximately 20 km from Yucca Mountain, a potential site for a high-level radioactive waste repository. The earthquake involved predominantly down-to-the-southeast dip-slip motion with a small left-slip component on a steeply dipping, 70° , northeast-striking fault. The mainshock nucleated near the base of the aftershock zone and ruptured up and to the northeast, and the mainshock rupture and the majority of the aftershock sequence were confined to depths between 6 and 12 km. All three M_L 4+ (largest M_L 4.5) aftershocks occurred off the mainshock fault plane on secondary structures within the aftershock zone. The nearest strong-motion instrument located 11 km southwest of the epicenter recorded a peak acceleration of $0.206g$. The earthquake occurred adjacent to the Rock Valley fault zone within an area of prior concentrated background seismicity and near the intersection of several northeast-striking faults in the southern NTS that have experienced Quaternary motion.

Introduction

The 29 June 1992, Little Skull Mountain (LSM) earthquake (origin time 10 hr 14 min 22.47 sec UTC, latitude 36° N $43.16'$; longitude 116° W $17.76'$; depth 11.7 km) occurred approximately 20 km southeast of a potential site for a high-level radioactive waste repository at Yucca Mountain, Nevada (Fig. 1). The M_L values of 5.8 and 5.6 were determined by the University of Nevada–Reno Seismological Laboratory (UNRSL) and the National Earthquake Information Center of the U.S. Geological Survey (USGS), respectively.

In this study we isolate the geometry of mainshock faulting and other active structures within the LSM aftershock zone from relocated hypocenters and well-constrained short-period focal mechanisms. Several faults were involved in the aftershock sequence. The geometry of these structures is correlated, where possible, with mapped features in the south-central Nevada Test Site (NTS). Also, from the aftershock distribution, we establish constraints on the static stress drop and average displacement during mainshock faulting. Previous studies (Harmsen, 1994; Meremonte *et al.*, 1995) were limited to the early aftershock period whereas we have used data through the end of 1992 and additional portable instrument data was available. We have applied a slightly different location procedure than previous studies and have attempted to isolate only the highest quality aftershock locations from this larger 6-month-period data set.

The LSM earthquake produced down-to-the-southeast dip-slip motion, with a small component of left-slip on a

steeply dipping (~ 65 – 70°) northeast-striking fault. The mainshock nucleated at the base of the aftershock zone with rupture propagation up and to the northeast; and the mainshock fault surface, and almost the entire sequence, was confined between 6- and 12-km depth. None of the three largest aftershocks ($M_L > 4$) took place on the mainshock fault plane but on secondary structures within the aftershock zone. The closest strong-motion instrument located 11 km southwest of the LSM epicenter on a thick section of sediments at Lathrop Wells, Nevada, recorded a peak ground acceleration of $0.206g$.

The LSM sequence provides one of the few visual images and a sense of motion for subsurface structure in the region. Focal mechanisms have been calculated for earthquakes in the southern Great Basin since comprehensive seismic monitoring began in 1978 (see USGS Open-File Reports for the southern Great Basin Seismic Network, for example, Harmsen and Bufe, 1992; Harmsen, 1993). However, these earthquakes have not been associated with extensive sequences, and the ambiguities in the actual fault plane orientations often remain.

Several tectonic models have been proposed for the Yucca Mountain area in attempts to evaluate the seismic hazard from the surface expression of mapped Quaternary faults. Fridrich (1998) pointed out that several proposed kinematic models rely on buried structures with little physical evidence for their existence. Low-angle detachment faults

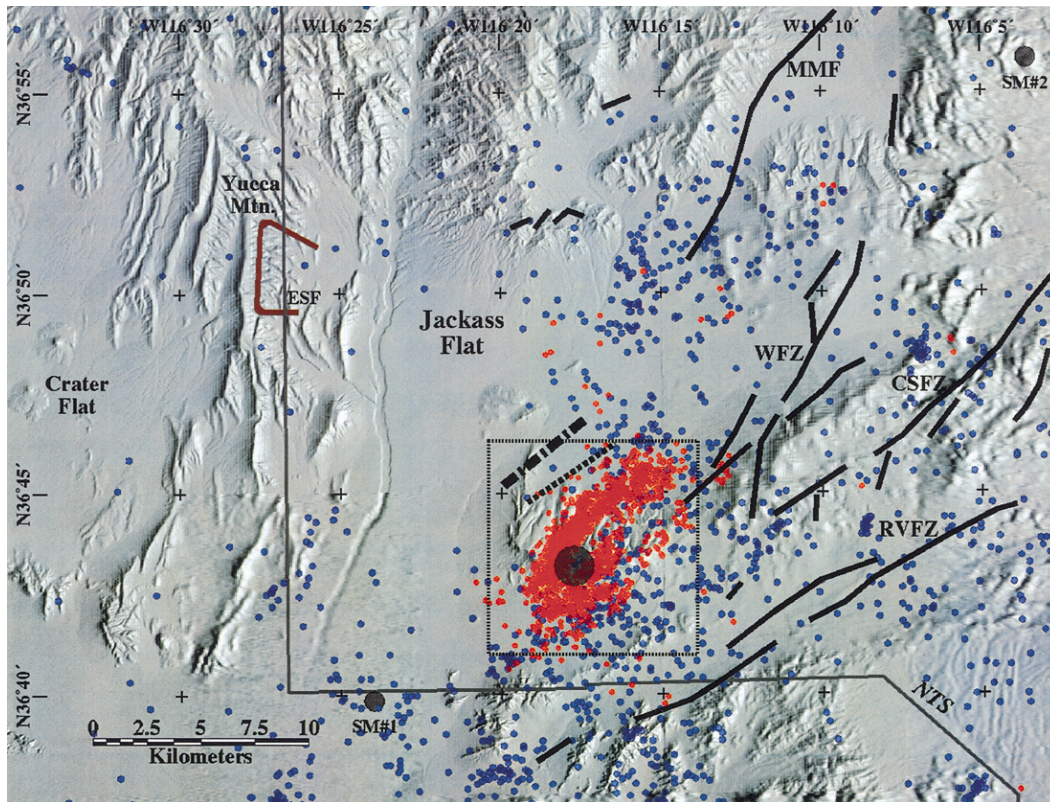


Figure 1. Shaded relief map of the LSM and Yucca Mountain regions. Rectangle bounds area of study shown in other figures. Labeled fault zones: MMFZ, Mine Mountain; WFZ, Wahmonie; RVFZ, Rock Valley; CSFZ, Cane Spring. SM#1 and SM#2 are locations of strong-motion instruments. ESF-Exploratory Studies Facility.

extending through Jackass Flat and beneath Yucca Mountain have been invoked to account for the tilting and the close spacing of normal faults in the Yucca Mountain block (Scott, 1990). Large-scale regional strike-slip faulting extending through Crater Flat has been proposed to address mapped offsets in Paleozoic facies (Schweichert, 1989).

Considering its proximity to the Yucca Mountain and the ongoing seismic hazard evaluation for the potential repository site, the LSM sequence is significant in providing a view of a normal faulting event and a wealth of ground-motion data. Harmsen (1994) and Meremonte *et al.* (1995) have reported on several aspects of the LSM sequence. Harmsen (1994) inferred the regional stress directions and preferred fault planes within the aftershock zone from a set of short-period focal mechanisms and a stress inversion routine. Meremonte *et al.* (1995) provided an interpretation of the geometry of faulting within the aftershock zone with respect to local mapped Quaternary faults using a limited set of robust hypocentral determinations. They (Meremonte *et al.*, 1995) also discussed the local geology and summarized deformation models in and around the LSM area.

The 1992 LSM earthquake is notable in several respects. It was the largest earthquake in the southern Great Basin since an M_L 5.7–6.1 earthquake near Caliente, Nevada, in

1966 (Meremonte and Rogers, 1987; Rogers *et al.*, 1991). It also has been the largest tectonic event within 50 km of Yucca Mountain in historical times. The May 1993 M_L 6.1 Eureka Valley, California (Peltzer and Rosen, 1995) and the 1 August 1999, M_L 5.6 Scottys Junction, Nevada, earthquake have been the largest of the most recent events in the southern Great Basin. Other, more recent moderate-sized earthquakes in the southern Great Basin have included a series of M 5+ events near Ridgecrest, California, in the mid-1990s in southern Owens Valley (Hauksson *et al.*, 1995).

The LSM event was the largest earthquake of an unprecedented pulse of seismicity that was recorded throughout the Basin and Range following the 28 June 1992 M_s 7.5 Landers, California, earthquake. This unusual short-term increase in earthquake activity, as well as the LSM earthquake itself, was most likely triggered by the Landers event (Anderson *et al.*, 1993; Hill *et al.*, 1993; Bodin and Gomberg, 1994; Gomberg and Bodin, 1994). Although the LSM earthquake took place 20 hr following Landers, earthquake activity in the LSM source region was detected within the coda of the Landers event providing the best evidence for a direct triggering mechanism (Anderson *et al.*, 1994; Gomberg and Bodin, 1994).

A mapped structure with Quaternary offsets that is clos-

est to the epicenter of the LSM earthquake is the northeast-striking Rock Valley fault zone (RVFZ; Fig. 1), although the LSM earthquake did not occur in the RVFZ. The RVFZ is adjacent to and south of the LSM and extends in an east-northeast direction from the western Specter Range through the eastern part of the NTS (Stewart and Carlson, 1978; Stewart, 1980; Carr, 1984, 1990; Scott, 1990; O'Leary, 2001). Its Quaternary history is characterized by high-angle left-lateral strike-slip faulting on several individual segments (O'Leary, 2000). The RVFZ is one of the several mapped, generally northeast-trending, fault zones in the south-central NTS (Carr, 1984), including the Cane Spring, Wahmonie, and Mine Mountain systems (Fig. 1). There has been a notable increase in earthquake activity in the RVFZ since the LSM sequence, suggesting that the LSM event may be in some way related to this increase in RVFZ area seismicity. This activity has included a sequence of several hundred earthquakes at unusually shallow depths in 1993, in addition to several other M 3.5+ events over the past several years (Smith *et al.*, 2000). An M 4.7 event occurred in the Frenchman Flat area in January 1999. Since the Frenchman Flat event and sequence there has been a general decrease in seismicity rates to pre-LSM levels. Figure 1 also shows earthquake activity from the SGBSN catalog from 1978 to just prior to the LSM earthquake.

LSM Mainshock

Table 1 (J. Schneider, 1995, personal comm.) summarizes the seismic moments and focal mechanisms for the mainshock from various sources. An M_L of 5.8 (± 0.2) was estimated from the UNRSL regional digital network (Savage and Anderson, 1995), and NEIC reported an M_L of 5.6. The short-period P -wave first-motion focal mechanism as well as an interpretation of the preferred fault plane based on the aftershock geometry is shown in Figure 2. The focal mechanisms of the mainshock and the 5 July M 4.4 and 13 September M 4.5 aftershocks shown in Figure 2 were determined with FPFIT (Reasenber and Oppenheimer, 1985).

The orientations of the fault planes of the mainshock mechanism are well constrained by Pn readings at regional distances. The preferred fault plane (dashed in Fig. 2) dips steeply to the southeast and is based on the distribution and alignment of early aftershock activity (discussed subsequently). The mainshock involved primarily normal displacement with a small left-slip component (T axis: strike N135°E, plunge: 68°, P axis: strike N359°W, plunge 30°).

Meremonte *et al.* (1995) suggested that the LSM earthquake occurred on a southwestward extension of the Mine Mountain fault zone (MMFZ). This interpretation is based on an apparent alignment with the MMFZ and lineations in potential field data from previous studies. Evidence for an extension of the MMFZ through the Jackass Flat is limited to potential field data, and Quaternary activity along the MMFZ is only documented along its northern part (Piety, 1996). From a dip of 70° and a hypocentral depth of 11.8 km de-

Table 1
Mainshock Focal Mechanism and Moment Estimates*

Source	Strike	Dip	Rake	M_0 ($\times 10^{24}$ dyne/cm)
This study	60 \pm 15	70 \pm 13	-70 \pm 10	—
Meremonte <i>et al.</i> (1995)	55	56	-72	—
Romanowicz <i>et al.</i> (1993)	43	66	-73	3.5
Romanowicz <i>et al.</i> (1993)	34	44	-70	2.6
Zhao and Helmberger (1994)	45	55	-60	3.0
Walter (1993)	35	54	-87	4.1
Harmsen (1994)	55	56	-72	—

*From J. Schneider, 1995, personal comm.

termined in this study, the LSM fault plane projects to the surface in southern Jackass Flat, south of the mapped projections of the MMFZ (Fig. 1). This orientation results in an alignment intermediate between the strike of the RVFZ and the MMFZ. Also, the MMFZ, Cane Spring, Wahmonie, and RVFZs converge near the LSM aftershock zone. This could as well be a zone of complex deformation with intersecting faults of a variety of orientations not clearly associated with any one particular structure. Also, the hanging-wall block of the LSM event is topographically higher than the footwall, defining a structure with minimal total offset since the Miocene. If this is an extension of normal faulting within the MMFZ there has been little cumulative displacement at its southern end. An M 3.9 event in 1998 in northern Jackass Flat showed right-lateral strike-slip motion on a northwest-striking structure that would tend to truncate the MMFZ in the central Jackass Flat. To more confidently associate the LSM event with the MMFZ, with the implication that the MMFZ shows Holocene activity and is nearly twice its current length, may require more detailed geologic and geophysical studies in the southern Jackass Flat.

A 30-station strong-motion network was in operation in southern Nevada at the time of the LSM event (Lum and Honda, 1992). The closest station was 11 km southwest of LSM at Lathrop Wells, Nevada (SM#1; Fig. 1). A peak acceleration of 0.206g was recorded on the east-west component at this station (Fig. 3). The next closest instrument, SM#2, 30 km northeast of the earthquake measured a PGA of 0.150g (Fig. 3). The narrowing of the S -wave train at SM#2, relative to that observed for SM#1, is most likely due to rupture directivity along this source to receiver azimuth. The location of the mainshock hypocenter at the southwestern extent of the aftershock zone (Fig. 2) is consistent with unilateral rupture propagation to the northeast, toward SM#2. Figure 3 includes the S -wave acceleration spectra for both the horizontal components of ground motion at SM#1 and SM#2, respectively. The highest accelerations were experienced in the 2- to 10-Hz band. The difference between the SM#1 and SM#2 spectra at high frequencies is most likely due to differences in the site conditions; SM#1 is located on a thick section of Quaternary alluvium and SM#2 is a hard rock site.

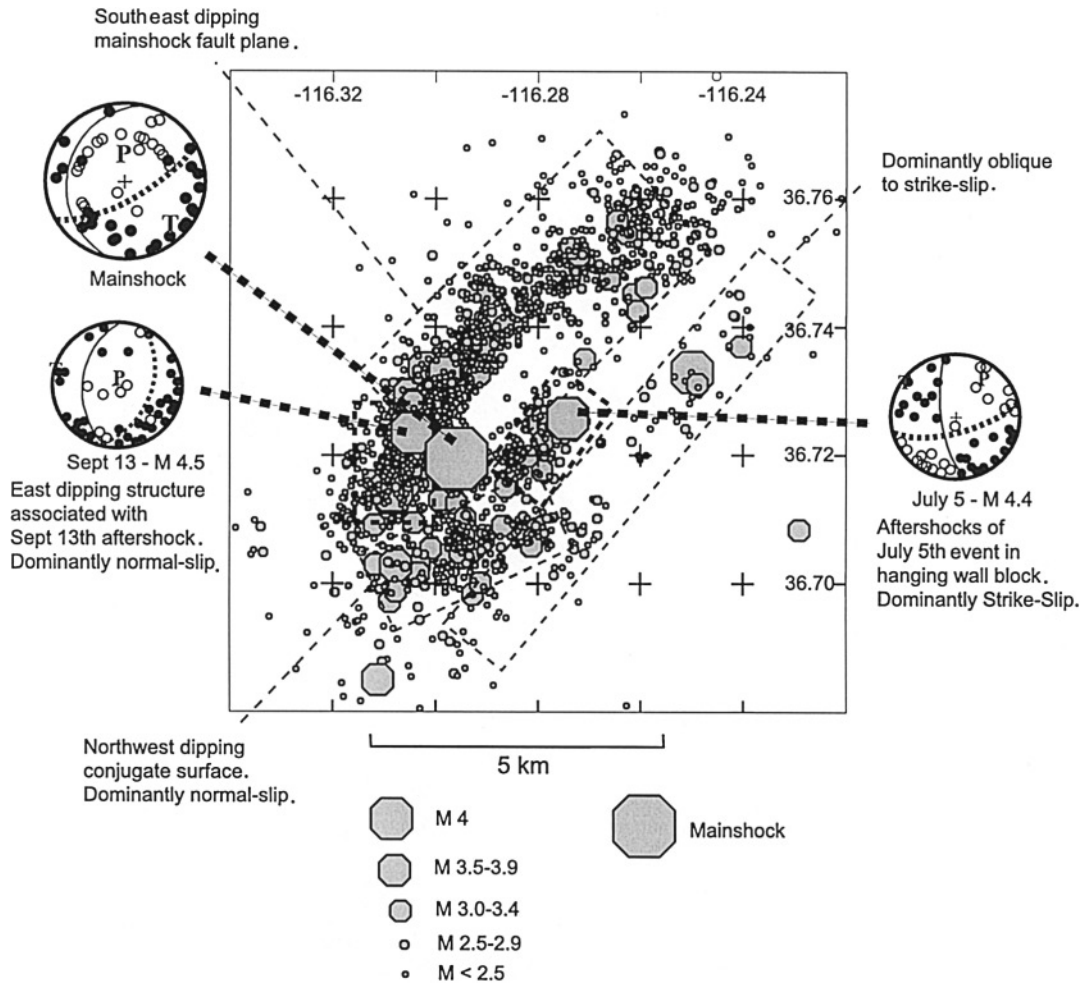


Figure 2. LSM earthquake activity, June–December 1992. Plotted are events that meet criteria for good location quality.

Earthquake Relocations and Focal Mechanism Determination

The LSM earthquake sequence took place in the transition of SGBSN operations from the USGS to the UNRSL. Each group operated portable seismic instruments during the early part of the LSM sequence, and the UNRSL operated a portable array through December 1992. As a result, data used for the analysis of this sequence come from several sources covering various time periods. We have integrated the data sets to provide as much control as possible on aftershock locations and focal mechanisms.

Data

Data from the SGBSN, through 1 October 1992, were processed in Golden, Colorado (Harmsen, 1993). The USGS has published yearly Open-File Reports since 1978 on the operations of the SGBSN, which describe the data recording. The UNRSL began operation of the network in September

1992. Analog data from the LSM sequence were transmitted by microwave to the University of Nevada campus in Reno, Nevada, and processed through the CUSP system (Peppin and Nicks, 1992). At the time of the LSM earthquake the SGBSN consisted of single-component vertical 1-Hz seismometers with horizontal components at some stations. The network is operated at a high gain in order to increase the magnitude detection threshold, but several horizontal components are operated at a lower gain to ensure on-scale horizontal-component records for amplitude magnitude determinations (Gomberg, 1991; Harmsen, 1993).

The M_L determined from a low-gain horizontal component at a station on LSM (SGBSN station, LSM) was assigned to earthquakes in the June–August time period (S. Harmsen, 1992, personal comm.). Magnitudes from September to the end of 1992 were determined by the UNRSL using a duration magnitude scheme. During September 1992 both groups operated the SGBSN to provide some consistency in location and magnitude estimates through the transition period. The UNRSL duration magnitudes, which were compared with USGS M_L measurements for the September time

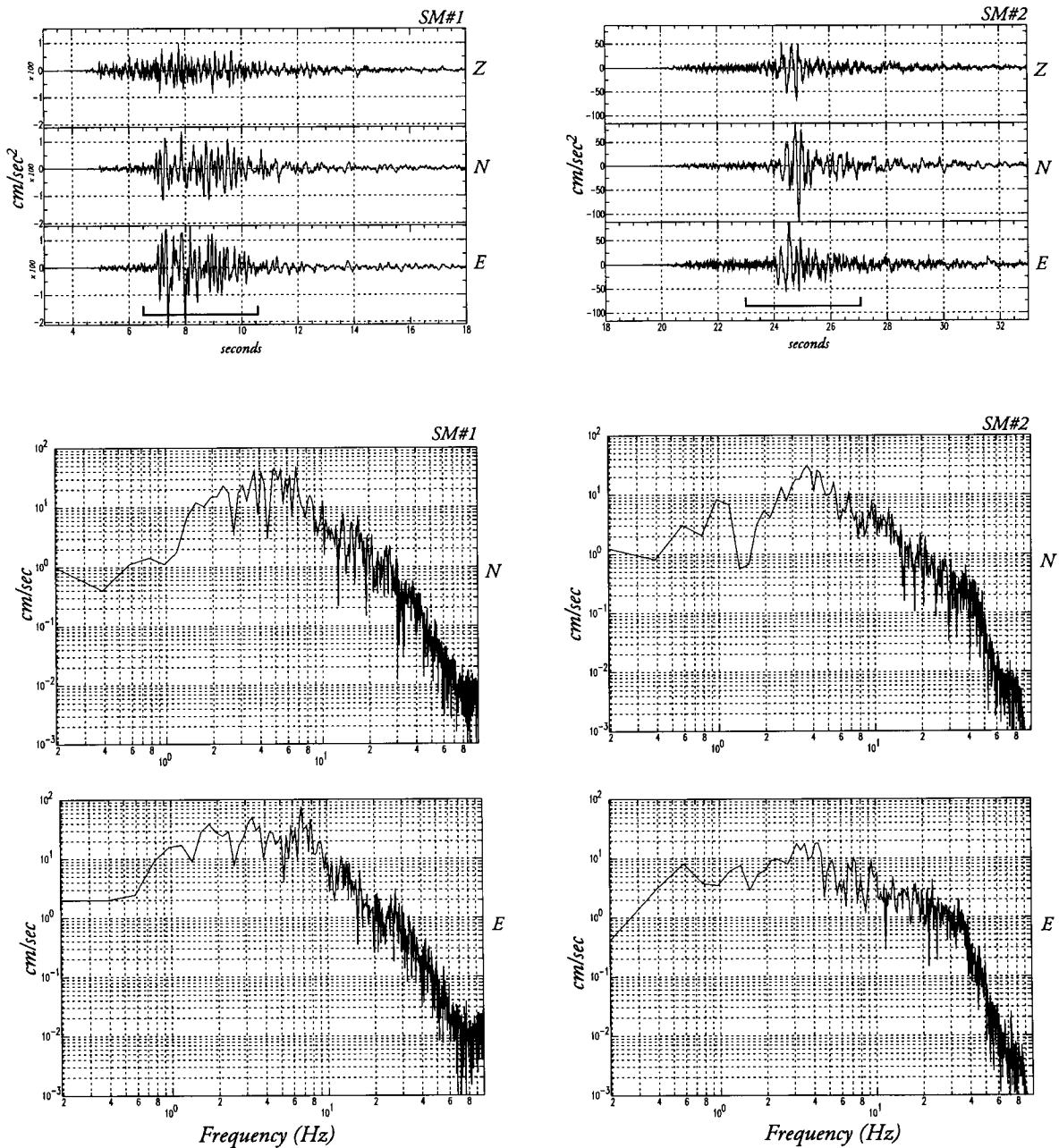


Figure 3. Acceleration time series and horizontal component S-wave acceleration spectra of the LSM earthquake at strong-motion stations SM#1 (left) and SM#2 (right).

period, generally agree to within 0.1 magnitude units (D. von Seggern, 1992, personal comm.).

Approximately 3800 earthquakes were detected within the SGBSN during the LSM aftershock sequence from June to December 1992. On a few occasions, first-arrival times were determined from the optical backup records due to down time in the data acquisition system. This was the case for the LSM mainshock, LSM foreshocks, and the first few hours of aftershock activity and other specific times reported by Meremonte *et al.* (1993). Arrival times can be resolved to about 0.1 sec from optical records, whereas an accuracy

of 0.01–0.02 sec is typical for near-source 100-Hz digital recordings. Where necessary, first motion readings from optical records have been included (S. Harmsen, 1992, personal comm.).

Earthquake Relocation

Arrival times from the regional network and portable instruments were associated to create the first-arrival database. Earthquakes were located with program FASTHYPO (Herrmann, 1979) using the following variation of the one-

dimensional velocity model of Hoffman and Mooney (1984) for the Yucca Mountain area (Table 2).

Hoffman and Mooney (1984) determined an average P -wave velocity of 3.0 km/sec for a 1-km-thick surface layer. We have modified this to 5.85 km/sec to account for larger S -wave travel-time residuals from near-source stations when using the slower surface velocities. This difference may be due to the high-velocity near-surface volcanic rocks at LSM. In order to develop a set of station corrections for network and portable instruments in the LSM area, only those events with more than 15 P -wave arrivals within 75 km of the aftershock zone were initially located. About 1700 events with 25,000 individual phase arrival times were used.

Average travel-time residuals were determined for each station from the suite of P -wave residuals with respect to the above one-dimensional velocity model and were relocated. Event rms residuals decreased significantly following relocation (rms event residuals decreased by an average of 0.15–0.08 sec). Meremonte *et al.* (1995) applied a similar method.

In order not to obscure the details of the aftershock distribution, only those earthquake locations that met particular, but reasonable, statistical location criteria are shown in the figures. These constraints are as follows: an rms residual of less than 0.1 sec, a location gap of less than 120° , and 10 or more stations within 75-km epicentral distance used in the location. Absolute location errors are estimated to be less than 1 km in the horizontal dimension and less than 2 km in depth, although we feel that the relative location accuracy is within several hundred meters. These error estimates are based on the average rms residuals. Focal mechanisms were determined for all events with more than 15 P -wave first-motion arrivals, and this resulted in 517 events that returned unique mechanism solutions (greater uncertainty can result in multiple solutions).

Aftershock Distribution, Mainshock Source Parameters, Focal Mechanism Distribution, and Foreshock Activity

Aftershock Distribution

Relocated LSM aftershocks show faulting on several structures, with most aftershock activity confined to the mainshock fault plane. However, a majority of the moment release in the aftershock period was dominated by three M_L 4+ earthquakes, none of which occurred on the mainshock fault plane. Figure 2 is an epicentral map of all earthquake activity in the LSM area that followed the Landers earthquake through the end of December 1992. Only good-quality events are included. The rectangle that encompasses the sequence of Figure 1 is the area covered in Figure 2. The mainshock is the large symbol at the southwest end of a northeast-trending elliptical-shaped area, in map view, that is generally free of aftershock activity. The three M_L 4+ events and the largest aftershocks occurred during this period. The first of these occurred immediately following the

Table 2
Velocity Model

Depth (km)	Velocity (km/sec)
0	5.85
1	6
25	6.35
30	6.6
35	7.8

mainshock, and its focal mechanism is poorly constrained. The M_L 4+ event of 5 July (0654 13.27 UTC; Fig. 2) occurred approximately 2-km northeast of, and 6 days following, the mainshock. (Latitude: 36° N $43.55'$; longitude: 116° W $16.46'$; depth: 9.39 km. Fault plane parameters: strike $N75^\circ$ E, dip 70° E, rake -20° ; T axis: strike $N30^\circ$ E, plunge 89° ; P axis: strike $N34^\circ$ W, plunge 62°). This event was followed by its own localized aftershock sequence in the hanging-wall block of the mainshock fault plane. The third M_L 4+ aftershock (13 September, 1146 20.87 UTC) occurred within the dense cluster of activity less than 1 km west of the mainshock epicenter (Fig. 2). (Latitude: 36° N $43.41'$; longitude: 116° W $18.28'$; depth 8.93 km. Fault plane parameters: strike $N20^\circ$ E, dip 45° SE, rake -80° ; T axis: strike $N283^\circ$ E, plunge 90° ; P axis: strike $N16^\circ$ W; plunge 70°).

Early Aftershock Activity—Mainshock Source Parameters

Except for the strike-slip faulting associated with the 5 July M_L 4+ event all major features within the aftershock distribution developed in the first 38 hr of the sequence (Fig. 4). The cross section of Figure 5 illustrates what we interpret to be the mainshock fault plane, striking $N48^\circ$ E and dipping 66° to the southeast. This is a 12° counterclockwise offset relative to the orientation of the mainshock fault plane from the short-period mechanism, but inasmuch as the mechanism represents only the initiation of faulting, these estimates may not necessarily be identical. Because very few earthquakes were located at shallow depths only the 5- to 13-km depth range is shown in Figure 5. Moreover, the shallowest aftershocks tended only to occur above the northeast end of the mainshock fault plane.

Figure 5 also shows the orientation of a fault surface that is conjugate to the mainshock fault plane. This structure dips approximately 45° to the northwest and is not consistent with the orientation of the auxiliary fault plane of the mainshock mechanism and is not aligned with the mainshock hypocenter. Therefore, we do not see evidence that this is the mainshock fault plane. It is difficult to isolate all structural features with cross-sectional views, but the focal mechanisms of this particular group of earthquakes suggest down-to-the-northwest normal motion on this feature (discussed subsequently).

We interpret the semicircular distribution of early after-

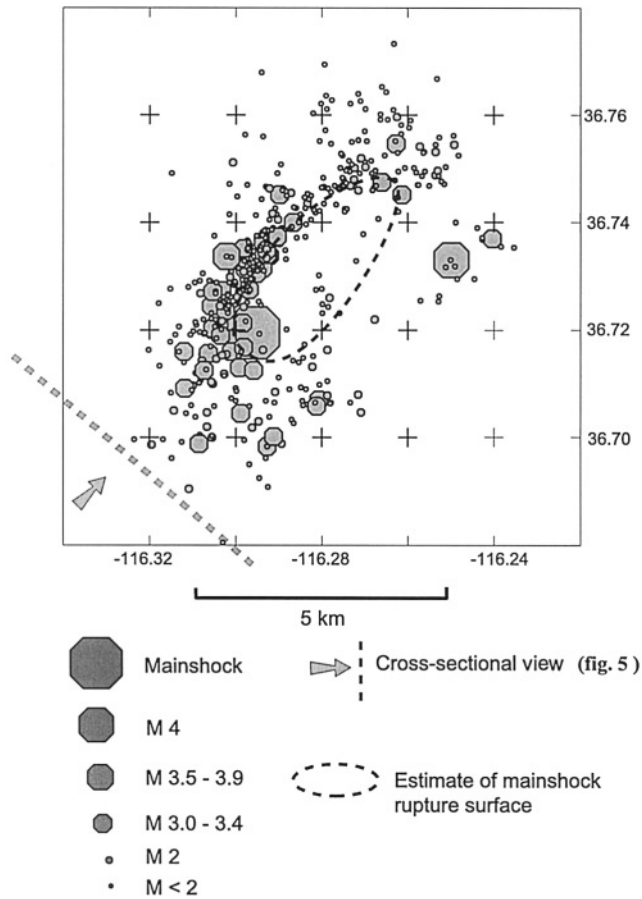


Figure 4. First 38 hr of aftershock activity. Cross-sectional view is given in Figure 5, and perspective view is shown in Figure 6.

shock activity west, north, and northeast of the mainshock hypocenter to represent the upper boundary of the mainshock slip surface (Fig. 2). Deeper events on this structure that plot within 3-km (epicentral distance) northeast of the mainshock outline this area at depth. These deeper earthquakes were confined to the first 38 hr of the sequence, whereas aftershock activity defining the upper portion of the interpreted rupture surface continued throughout the sequence. The lack of aftershocks within this proposed slip surface suggests nearly complete stress release on this fault surface during the earthquake.

The elliptical region in plan view in Figure 4 and in projection in Figure 6 roughly approximates a circular surface with radius (r) between 2.5 and 3.0 km. The stress drop ($\Delta\sigma$) for a circular fault (Brune, 1970; Aki and Richards, 1980) is given by

$$\Delta\sigma = \frac{7}{16} \frac{M_0}{r^3}.$$

Static stress drops and average displacements for the LSM event are shown in Table 3 for a range of source radii and published moments.

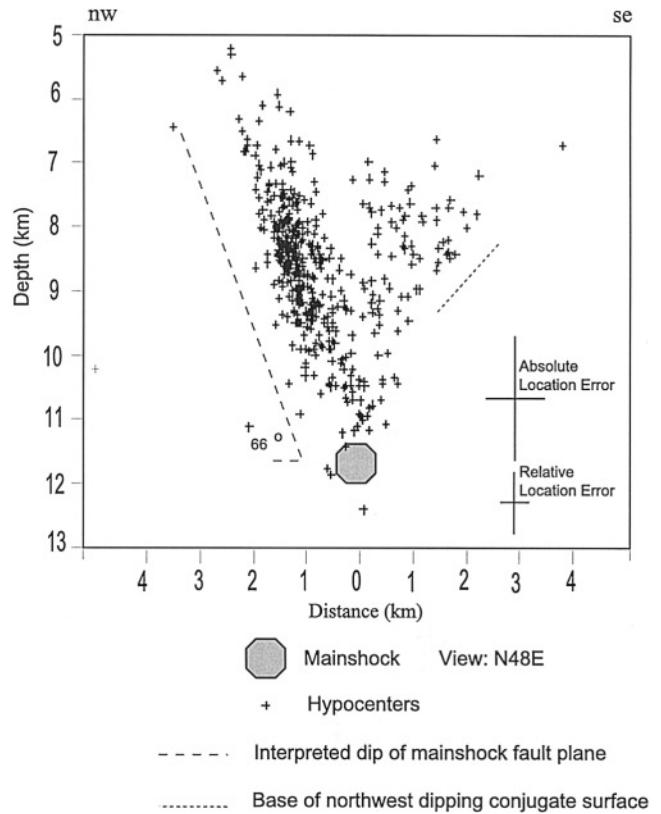


Figure 5. Cross-sectional view showing dip of the mainshock fault plane and early off-fault aftershock activity in the depth range 5-13 km.

A source radius of 2.5 km most closely approximates the area that is free of aftershock activity (Figs. 4, 6), whereas a 3-km radius includes most of the activity at the southwest and northeast ends of the aftershock zone. The interpreted rupture area in Figures 4 and 6 may be better approximated by an ellipse rather than a circle, which would decrease our estimates of the rupture area and thereby increase the static stress drop estimate. These estimates are based on the assumption that the distribution of aftershocks is directly related to the extent of faulting during the main event. Mayeda and Walter (1996) calculated a stress drop of 196 bars for the LSM earthquake based on the radiated energy at regional stations. These static stress drop estimates are high compared to stress drop estimates for California earthquakes. A thorough analysis of the LSM source is being conducted in other Yucca Mountain studies and is beyond the scope of this report.

There have been very few near-source studies of the source parameters of normal faulting events in the Basin and Range province. Boatwright (1985) determined the static stress drops of aftershocks of the Borah Peak earthquake, but no near-source waveforms were available for the mainshock. At Borah Peak, aftershock stress drops fell into two general ranges of 35 and 77 bars depending on the location of the event within the aftershock zone. Ichinose *et al.* (1997)

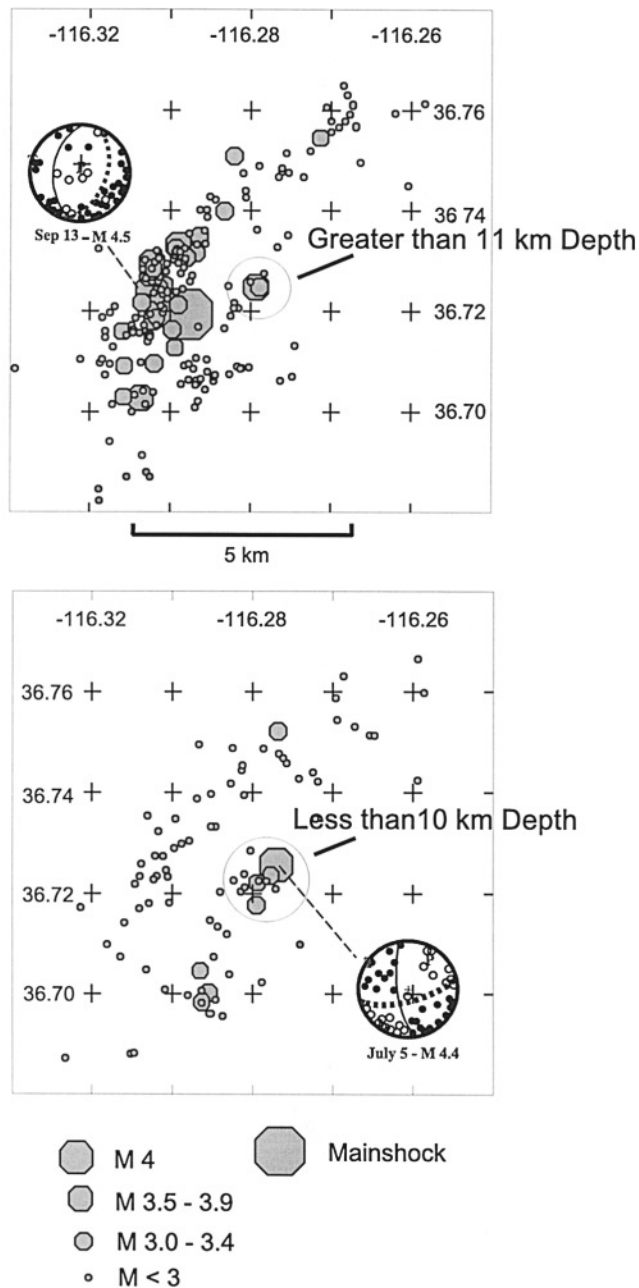


Figure 6. Spatial distribution of normal-slip (top) and strike-slip (bottom) short-period focal mechanisms.

estimated a stress drop of 60 bars for the magnitude 4.5 main event of the 1995 Border Town, Nevada, sequence. Mayeda and Walter (1996) found no significant difference between the stress drops of normal and strike-slip events but the data set for normal faulting events is limited. Clearly, understanding the unique aspects of the source processes for normal faulting events is important to understanding the seismic hazard in the extensional environment at Yucca Mountain.

The dense concentration of aftershocks west of the mainshock epicenter, which defines the western extent of the sequence (Fig. 2), indicates a high level of activity in the

Table 3
Mainshock Source Parameters

Seismic Moment ($\times 10^{24}$ dyne/cm)	Reference	Source Radius (km)	Stress Drop (Bars)	Fault Slip (cm)
4.1	Walter (1993)	2.5	114	69
4.1	Walter (1993)	2.75	86	57
4.1	Walter (1993)	3	66	48
5.5	Harvard CMT	2.5	154	93
5.5	Harvard CMT	2.75	115	77
5.5	Harvard CMT	3	89	64

early aftershock period (Fig. 4). This area shows predominantly normal faulting (Figs. 2 and 7) defining an east-dipping structure that includes the 13 September event. Consistent with these focal mechanisms the trend in the aftershock distribution in this locality is generally north-south, in contrast to the northeast-striking trend of activity that conforms to the mainshock fault plane. This north-south-striking structure would intersect the mainshock fault plane at a high angle and would therefore limit or truncate its western extent. Although aftershocks of the 13 September M_L 4+ event dominate the later aftershock period, this north-south-striking structure was active at the M 3+ level immediately after the mainshock (Fig. 4). In contrast to the east-dipping character of this fault surface, north-striking middle Tertiary normal faults on LSM show a down-to-the-west geometry similar to faults in the central Yucca Mountain block (Frizzell and Shulters, 1990; Day *et al.*, 1998).

The presence of the east-dipping structure discussed previously suggests another interpretation for displacement during the LSM mainshock: coseismic slip occurred on this structure, imposing a small component of down-to-the-northeast displacement of the hanging-wall block. The small component of left-slip in the mainshock focal mechanism (Fig. 2) may be an expression of this contribution to the faulting mechanism. This hypothesis may be difficult to test from regional records; slip on the east-dipping fault surface would exhibit a different focal mechanism than the mainshock, and the moment release on the subsidiary structure would be, at the most, only 15-20% of that on the northeast-striking mainshock fault plane.

Activity that forms the southeastern extent of the aftershock distribution includes the 29 June M 4+ event and several other M 3+ earthquakes (Figs. 2 and 4). In map view this activity extends between LSM and Skull Mountain and may represent reactivation of mapped middle Tertiary faults or a southern extension of the Wahmonie fault zone. Activity along this northeast trend is dominated by strike-slip and oblique-slip focal mechanisms (Fig. 7) and does not exhibit a wide depth distribution (Fig. 5).

Focal Mechanism Distribution

Figure 6 summarizes the spatial distribution of 89 strike-slip and 198 normal-slip focal mechanisms; only those

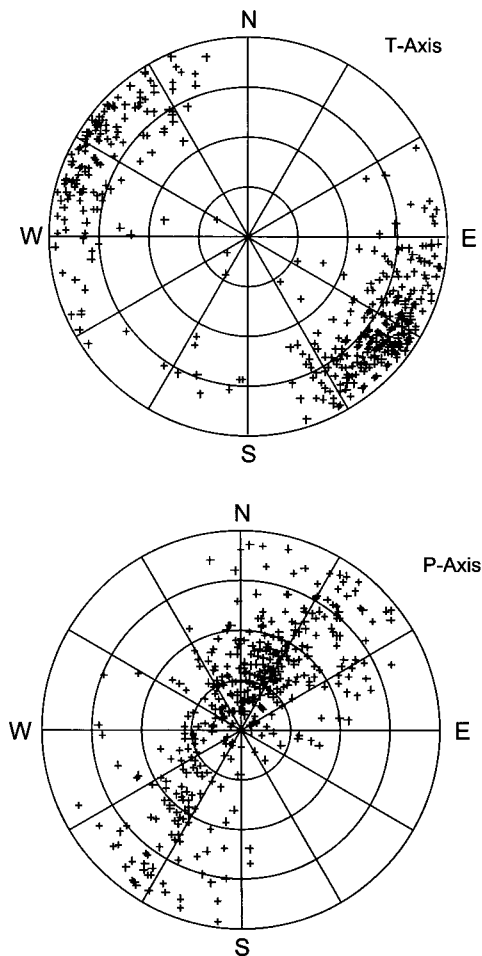


Figure 7. Lower hemisphere composite P - and T -stress axis distributions.

events with a T -axis inclination of less than 30° are plotted. In this figure, normal-slip events are defined as having a P -axis inclination greater than 60° (higher angles represent a more vertically oriented stress axis). Strike-slip events are those with a P -axis inclination of less than 30° . Oblique-slip events are not included in order to isolate the normal- and strike-slip deformation. Only one $M 3+$ strike-slip event is associated with the mainshock fault plane, and this event is at the northeast end of the aftershock zone. $M 3+$ normal-slip aftershocks conform to the mainshock fault plane and the east-dipping structure associated with the 13 September $M 4+$ aftershock. Normal faulting events that occur south of the mainshock are associated with the generally north-northwest-dipping feature that appears to intersect the mainshock fault plane that was discussed previously with reference to the early aftershock period (Figs. 2–6).

A cluster of strike-slip events associated with the 5 July $M 4$ earthquake trends generally northeast–southwest (Fig. 7). The 5 July earthquake and its aftershock sequence lie above a depth of 10 km and are confined to the hanging-wall block of the mainshock fault surface. A group of normal

faulting events in this same epicentral area occur below a depth of 11 km and are at the base of the southeast-dipping mainshock fault plane (Fig. 4). The preferred fault plane from the focal mechanism for the 5 July event and its aftershocks is therefore subparallel to the mainshock fault plane. Harmsen (1994) suggests the 5 July earthquake is a right-slip event, but we prefer the northeast-striking fault plane because of the general northeast aftershock alignment.

Based on an alignment of north-northeast-oriented high-angle right-slip fault planes in the region of the 5 July earthquake, Harmsen (1994) and Meremonte *et al.* (1995) suggested that some of this activity might be in the Wahmonie fault zone. We see little direct evidence for right-lateral strike-slip faulting in the LSM data. To support the argument for the sense of motion during the 5 July event and related aftershocks we also point out that this structure is subparallel to the trend of the RVFZ (Fig. 1), a predominantly high-angle left-slip structure. Activity on the structure associated with the 5 July event more clearly defines a northeast alignment by including aftershock data through the end of 1992.

Figure 7 shows lower-hemisphere composite P and T diagrams from the 517 unique solution focal mechanisms covering the LSM sequence. The average azimuth of the T axes is $N62^\circ W$, and Harmsen (1994) reported an average T -axis direction of $N60^\circ W$. These values are consistent with other studies of the orientation of the stress field in the southern Great Basin (Rogers *et al.*, 1987; Harmsen and Bufe, 1992). The average T -axis orientation is rotated 20° counterclockwise with respect to the azimuth of the T axis determined for the mainshock from this study. It can be deduced from the P -axis distribution that there are a number of strike-slip events, but normal-slip was the dominant sense of motion throughout the aftershock sequence. A few low-angle mechanisms in the LSM set, representing a small fraction of the total moment release, show no consistent spatial pattern similar to that shown by the strike-slip and normal-slip events and cannot be interpreted in terms of through-going low-angle structures. It is not unusual to observe some low-angle extensional or reverse-slip focal mechanisms in Basin and Range aftershock sequences.

Foreshocks

The source region of the LSM earthquake was active immediately following the 28 June 1992 $M_s 7.5$ Landers, California, earthquake. A microearthquake array operating at the Yucca Mountain (Brune *et al.*, 1992), 20 km west of LSM, detected a marked increase in microearthquakes at LSM immediately following the Landers event ($S - P$ times were consistent with the distance to LSM for the entire set). On the basis of this evidence, Anderson *et al.* (1994) and Gomberg and Bodin (1994) suggested that the LSM earthquake was dynamically triggered by surface waves generated by the Landers earthquake, although other physical processes for triggering of the LSM event have also been proposed (Bodin and Gomberg, 1994).

Figure 8 shows the cumulative number of events re-

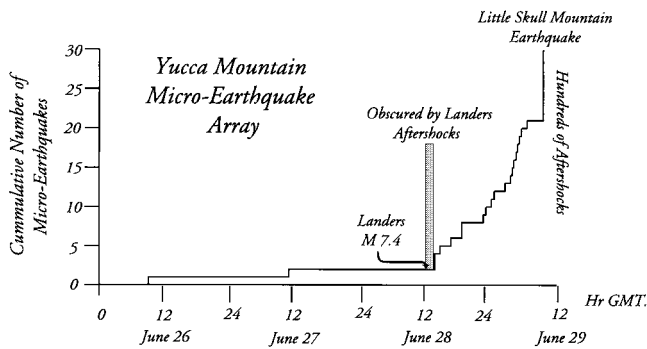


Figure 8. Cumulative microseismic activity from the LSM source region prior to the mainshock event (figure from Anderson *et al.*, 1994).

corded on a high-gain seismograph station located near Yucca Mountain prior to the LSM mainshock. Twelve of these events, including one $M 3+$ event, could be located with SGBSN data within the coda of Landers aftershock activity (Fig. 9). No microearthquake activity was observed on faults within the immediate vicinity of Yucca Mountain during the LSM foreshock period or LSM postseismic activity.

Summary and Conclusions

Although the LSM earthquake is a dominantly normal-slip event, it does not conform to the classic range front normal-faulting geometry that characterizes the Basin and Range province. In contrast to typical Basin and Range style normal-fault geometry, the hanging-wall block, crest of LSM, is topographically higher than the footwall. Because no expression of Quaternary faulting has been recognized near the surface projection of the LSM mainshock fault plane in Jackass Flat, this particular structure has experienced very little displacement throughout the Tertiary. Several other recent moderate sized earthquakes in the Basin and Range have not been associated with mapped faults, and this observation is not unusual.

Evidence for the steeply dipping geometry of the mainshock fault plane from well-located aftershocks and the short-period focal mechanism places the surface expression of the LSM earthquake southeast of that shown by Meremonte *et al.* (1995). Based on a general alignment they suggested that the LSM event may have occurred on a southwestern extension of the MMFZ (O'Leary, 2000). If this is a southern extension of the MMFZ, based on the observation that the hanging wall has greater relief than the footwall, this section of the fault has very little cumulative offset.

From the geometry of the structures within the aftershock zone the mainshock appears to have been initiated at the intersection of the southeast-dipping mainshock rupture plane and a northeast-striking high-angle fault, which is possibly a southwest extension of the Wahmonie or even Cane Spring fault zones. This is also suggested by Meremonte *et al.* (1995). Mapped expressions of the Mine Mountain, Wah-

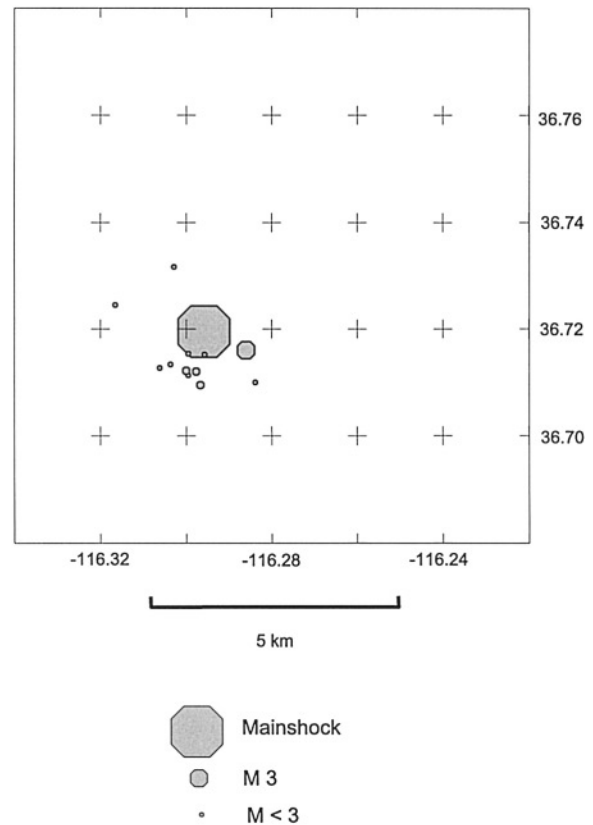


Figure 9. Location of LSM foreshock activity in the hours following the Landers earthquake.

monie, and Cane Spring all trend into the RVFZ in the LSM source region, and isolating one of these faults in the LSM area may be problematic. This may be a focal point for increased stress concentration, as illustrated by the concentration of pre-LSM seismicity (Fig. 1), which may indeed be the consequence of the interaction of these south-central NTS structures. Because the RVFZ is the most active of these structures it seems reasonable to propose that the LSM event may have been influenced by deformation associated with the RVFZ rather than the MMFZ.

No $M 4+$ LSM aftershocks took place on the mainshock fault plane, but such events occurred on subsidiary structures within the aftershock zone. A set of aftershocks directly west of the mainshock epicenter aligns along a distinct northerly trend. This alignment is consistent with the normal-slip focal mechanism of the 13 September $M_L 4+$ event and a number of normal-slip aftershocks. The preferred fault plane for the $M 4+$ 13 September event strikes nearly north-south and dips to the east. Near the epicenter of the latter event the aftershock distribution defines an intersection between the southeast-dipping mainshock fault plane and this east-dipping structure. This is also the location of LSM foreshock activity and the point of initiation of mainshock rupture.

The time of the initiation of foreshock activity suggests that the LSM earthquake was triggered by surface wave energy generated during the 28 June Landers, California, event

(Anderson *et al.*, 1994). Microearthquake activity in the LSM source region was observed immediately following the Landers event with foreshock activity continuing to the time of the LSM mainshock. Because of its close proximity to the Yucca Mountain the LSM earthquake and aftershock sequence have been particularly important for ongoing seismic hazard studies.

A fundamental observation about the LSM is that the 9-Ma basalt surface that caps the mountain dips to the north in contrast to the fairly flat lying stratigraphy on Skull Mountain to the east. This clearly means that some northward rotation/tilt of the LSM block into the Jackass Flat has taken place since the late Miocene. The rotation is consistent with collapse of the Jackass Flat basin, and the LSM event may be reflecting this process. If this is occurring, then the Jackass Flat may consist of several LSM-type normal faults or grabens distributed throughout the basin contributing to the basin collapse.

Acknowledgments

Wally Nicks, Austin Wilson, and Charlotte Middlebrooks maintained operations of the SGBSN at the University of Nevada-Reno through the LSM sequence. John Perry maintained the portable array through the end of 1992. Stephen Gillett assisted to a large degree in the processing and organizing of the large amount of portable data that was collected during the sequence. We would also like to thank Steve Harmsen, Joan Gomberg, Ed Cranswick, Mark Meremonte, and Jim Brooks of the USGS for their help in the field deployment and for supplying their portable data.

References

- Aki, K., and P. Richards (1980). *Quantitative Seismology: Theory and Methods*, W. H. Freeman, New York.
- Anderson, J. G., J. N. Brune, D. dePolo, J. Gomberg, S. C. Harmsen, M. K. Savage, A. K. Sheehan, and K. D. Smith (1993). Preliminary report: the Little Skull Mountain earthquake, June 29, 1992, in *Dynamic Analysis and Design Considerations for HIGH-LEVEL Nuclear Waste Repositories*, Structural Division/American Society of Civil Engineers, New York, 162–175.
- Anderson, J. G., J. N. Brune, J. N. Louie, Y. Zeng, M. Savage, G. Yu, Q. Chen, and D. dePolo (1994). Seismicity triggered by the Landers, California, Earthquake, 28 June 1992, *Bull. Seism. Soc. Am.* **84**, 863–891.
- Boatwright, J. (1985). Characteristics of the aftershock sequence of the Borah Peak, Idaho, earthquake determined from digital recordings of the event, *Bull. Seism. Soc. Am.* **75**, 1265–1284.
- Bodin, P., and J. Gomberg (1994). Triggered seismicity and deformation between the Landers, California, and Little Skull Mountain, Nevada, earthquake, *Bull. Seism. Soc. Am.* **84**, 835–843.
- Brune, J. N. (1970). Tectonic stress and the spectra of seismic shear waves from earthquakes, *J. Geophys. Res.* **75**, 4997–5009.
- Brune, J. N., W. Nicks, and A. Aburto (1992). Microearthquakes at Yucca Mountain, Nevada, *Bull. Seism. Soc. Am.* **82**, 164–174.
- Carr, W. J. (1984). Regional structural setting of Yucca Mountain, Southwestern Nevada, and late Cenozoic rates of tectonic activity in part of the Southwestern Great Basin, Nevada and California, *U.S. Geol. Surv. Open-File Rept.* 84-854, 109 pp.
- Carr, W. J. (1990). Styles of extension in the Nevada Test Site region, Southern Walker Lane Belt: an integration of volcano-tectonic and detachment fault models, in *Basin and Range Extensional Tectonics Near the Latitude of Las Vegas, Nevada*, B. P. Wernicke (Editor), *Geol. Soc. Am. Memoir* 176, 283–303.
- Day, W. C., C. J. Potter, D. S. Sweetkind, R. P. Dickerson, and C. A. San Juan (1998). Bedrock geologic map of the central block area, Yucca Mountain, Nye County, Nevada, *U.S. Geol. Surv. Misc. Invest. Series Map I-2601*, scale 1:6000.
- Dokka, R. K., and C. J. Travis (1990). Role of the Eastern California shear zone in accommodating Pacific-North American plate motion, *Geophys. Res. Lett.* **17**, 1323–1326.
- Fridrich, C. J. (1998). Tectonic evolution of the Crater Flat basin, Yucca Mountain region, Nevada, *U.S. Geol. Surv. Open-File Rept.* 98-33, 30 pp.
- Frizzell Jr., V. A., and J. Shulters (1990). Geologic map of the Nevada Test Site, southern Nevada, *U.S. Geol. Surv. Misc. Invest. Series Map I-2046*.
- Gomberg, J. (1991). Seismicity and detection/location threshold in the Southern Great Basin Seismic Network, *J. Geophys. Res.* **96**, 16,401–16,414.
- Gomberg, J., and P. Bodin (1994). Triggering of the M_S 5.4 Little Skull Mountain, Nevada, earthquake with dynamic strains, *Bull. Seism. Soc. Am.* **84**, 844–853.
- Harmsen, S. C. (1993). Seismicity and focal mechanisms for the Southern Great Basin of Nevada and California in 1991, *U.S. Geol. Surv. Open-File Rept.* 92-340.
- Harmsen, S. C. (1994). The Little Skull Mountain, Nevada, earthquake of June 29, 1992: aftershock focal mechanisms and tectonic stress field implications, *Bull. Seism. Soc. Am.* **84**, 1484–1505.
- Harmsen, S. C., and C. G. Bufe (1992). Seismicity and focal mechanisms for the southern Great Basin of Nevada and California: 1987 through 1989, *U.S. Geol. Surv. Open-File Rept.* 91-572.
- Hauksson, E., K. Hutton, H. Kanamori, L. Jones, J. Mori, S. Hough, and G. Roquemore (1995). Preliminary report on the 1995 Ridgecrest earthquake sequence in eastern California, *Seism. Res. Lett.* **66**, 54–60.
- Herrmann, R. B. (1979). FASTHYPO: a hypocenter location program, *Earthquake Notes* **50**, 25–37.
- Hill, D. P., R. A. Reasenber, A. Michael, W. J. Arabaz, G. Beroza, D. Brumbaugh, J. N. Brune, R. Castro, S. Davis, D. dePolo, W. L. Ellsworth, J. Gomberg, S. Harmsen, L. House, S. M. Jackson, M. J. S. Johnston, L. Jones, R. Keller, S. Malone, L. Munguia, S. Nava, J. C. Pechmann, A. Sanford, R. W. Simpson, R. B. Smith, M. Stark, M. Stickney, A. Vidal, S. Walter, W. Wong, and J. Zollweg (1993). Seismicity remotely triggered by the magnitude 7.3 Landers, California, earthquake, *Science* **260**, 1617–1623.
- Hoffman, L. R., and W. D. Mooney (1984). A seismic study of Yucca Mountain and vicinity, Southern Nevada; data report and preliminary results, *U.S. Geol. Surv. Open-File Rept.* 83-588.
- Ichinose, G., K. D. Smith, and J. G. Anderson (1997). Source parameters of the 1995 Border Town, Nevada, earthquake sequence, *Bull. Seism. Soc. Am.* **83**, 652–667.
- Lum, P. K., and K. K. Honda (1992). Processed seismic motion records from Little Skull Mountain, Nevada, earthquake of June 29, 1992, recorded at stations in southern Nevada, National Technical Information Service, Report #JAB-10733-TM6 UC-703.
- Mayeda, K., and W. R. Walter (1996). Moment, energy, stress drop, and source spectra of western United States earthquakes from regional coda envelopes, *J. Geophys. Res.* **101**, 11,195–11,208.
- Meremonte, M., E. Cranswick, J. Gomberg, D. Worley, D. Carver, J. Brooks, R. Banfill, D. Overturf, and T. Bice (1993). Report on the seismological field investigations of the 29 June 1992 Little Skull Mountain earthquake, *U.S. Geol. Surv. Open-File Rept.* 93-555.
- Meremonte, M. E., J. Gomberg, and E. Cranswick (1995). Constraints on the 29 June 1992 Little Skull Mountain sequence provided by robust hypocentral estimates, *Bull. Seism. Soc. Am.* **85**, 1039–1049.
- Meremonte, M. E., and A. M. Rogers (1987). Historical catalog of Southern Great Basin earthquakes 1868–1978, *U.S. Geol. Surv. Open-File Rept.* 87-80.

- O'Leary, D. W. (2000). Tectonic significance of the Rock Valley fault zone, Nevada Test Site, *U.S. Geol. Surv. Open-File Rept. Seismic Hazard Issues Yucca Mountain* (in press).
- Peltzer, G., and P. Rosen (1995). Surface displacement of the May 17, 1993 Eureka Valley California earthquake observed by SAR interferometry, *Science* **268**, 1333–1336.
- Peppin, W. A., and W. F. Nicks (1992). Real time analog and digital data acquisition through CUSP, *Seism. Res. Lett.* **63**, 181–189.
- Piety, L. A. (1996). Compilation of known or suspected Quaternary faults within 100 km of Yucca Mountain, Nevada and California, *U.S. Geol. Surv. Open-File Rept. 94-112*.
- Priestley, K. F., K. D. Smith, and R. S. Cockerham (1988). The 1984 Round Valley, California earthquake sequence, *Geophys. J.* **95**, 215–235.
- Reasenber, P. A., and D. Oppenheimer (1985). FPFIT, FPLOT, and FPPAGE: Fortran computer programs for calculating and displaying earthquake fault-plane solutions, *U.S. Geol. Surv. Open-File Rept. 85-739*.
- Rogers, A. M., S. C. Harmsen, and M. E. Meremonte (1987). Evaluation of the seismicity of the Southern Great Basin and its relationship to the tectonic framework of the region, *U.S. Geol. Surv. Open-File Rept. 87-408*.
- Rogers, A. M., S. C. Harmsen, E. J. Corbett, K. F. Priestly, and D. dePolo (1991). The seismicity of Nevada and some adjacent parts of the Great Basin, in *Neotectonics of North America: Geological Society of America, Decade of North American Geology, Map, D. B. Slemmons, E. R. Engdahl, M. D. Zoback, and D. D. Blackwell (Editors), Vol. 1, 153–184*.
- Romanowicz, B., Dreger, M. Pasyanos, and R. Uhrhammer (1993). Monitoring strain release in the central and northern California using broadband data, *Geophys. Res. Lett.* **20**, 1643–1646.
- Savage, M. K., and J. G. Anderson (1995). A local magnitude scale for the western Great Basin-eastern Sierra Nevada from synthetic Wood-Anderson seismograms, *Bull. Seism. Soc. Am.* **85**, 1236–1245.
- Schweichert, R. A. (1989). Evidence for a concealed strike-slip fault beneath Crater Flat, Nevada, *Geol. Soc. Am. Abstr. Prog.* **21**, A90.
- Scott, R. B. (1990). Tectonic setting of Yucca Mountain, Southwest Nevada, in *Basin and Range Extensional Tectonics near the Latitude of Las Vegas, Nevada*, B. P. Wernicke (Editor), *Geol. Soc. Am. Memoir* **176**, 251–282.
- Smith, K. D., and K. F. Priestley (1988). The foreshock sequence of the 1986 Chalfant, California earthquake, *Bull. Seism. Soc. Am.* **78**, 172–187.
- Smith, K. D., J. N. Brune, and G. Shields (2000). A sequence of very shallow earthquakes in the Rock Valley fault zone, southern Nevada Test Site, *U.S. Geol. Open-File Rept. Seismic Hazard Issues Yucca Mountain* (in press).
- Stewart, J. H. (1980). *Geology of Nevada: Nevada Bureau of Mines and Geology Spec. Publ. 4*.
- Stewart, J. H., and J. E. Carlson (1978). *Geologic map of Nevada: Nevada Bureau of Mines and Geology Spec. Publ. 4 Suppl. scale 1:500,000*.
- Walter, W. (1993). Source parameters of the June 29, 1992 Little Skull Mountain Earthquake from complete regional waveforms at a single station, *Geophys. Res. Lett.* **20**, 403–406.
- Zhao, L. S., and D. V. Helmberger (1994). Source estimation from broadband regional seismograms, *Bull. Seism. Soc. Am.* **84**, 91–104.

Nevada Seismological Laboratory
MS 174
University of Nevada
Reno, Nevada 89557
(K.D.S.)

Manuscript received 22 June 2000.